



SHAPE MEMORY ALLOY CONFINED CONCRETE UNDER CYCLIC LOADING: EXPERIMENTAL TESTING AND MODELING

Q. Chen⁽¹⁾, B. Andrawes⁽²⁾

⁽¹⁾ Design Engineer, Skidmore, Owings & Merrill LLP, chen303@illinois.edu

⁽²⁾ Associate Professor, University of Illinois at Urbana-Champaign, andrawes@illinois.edu

Abstract

The idea of using shape memory alloy (SMA) spirals to apply active confinement to concrete prior to loading without the need for mechanical prestressing was first proposed in 2008 and previous studies show the promise of this new technique for seismic applications to significantly improve concrete strength and ductility. However, there is limited knowledge about the stress-strain behavior of SMA confined concrete and lack of robust analytical models that are able to predict three dimensional (3-D) behavior of concrete confined with SMA spirals under cyclic loading accurately. This research focused on addressing these knowledge gaps. A comprehensive experimental program is conducted on SMA confined concrete cylinders with different concrete strengths, spiral pitches and confining pressures to explore their effects on the stress-strain behavior of SMA confined concrete. Next, the experimental results are utilized to develop a new constitutive model for SMA confined concrete within the framework of Drucker-Prager plasticity model. The proposed constitutive model for SMA confined concrete is validated using experimental results. This model is able to take into account the unique behavior of SMA confined concrete, which involves a combination of both active and passive confinement, and is capable of simulating the 3-D stresses of SMA confined concrete.

Keywords: Shape Memory Alloys; Confinement; Concrete; Plasticity Model; Cyclic



1. Introduction

Concrete confinement has been proven as an effective approach to improve the ductility of reinforced concrete (RC) structures by numerous researchers (Richart *et al.* 1928; Sheikh and Uzumeri 1982; Mander *et al.* 1988; Imran and Pantazopoulou 1996). In recent years, an innovative confinement technique using shape memory alloy (SMA) spirals was proposed and studied by Andrawes and Shin in 2008 and proven to be promising for seismic retrofitting of concrete structures. Shin and Andrawes (2011) explored the application of using SMA spirals to retrofit RC columns to enhance their ductility and they demonstrated that active confinement provided by SMA spirals can effectively improve the ultimate strain and ultimate stress of concrete compared to passively confined concrete. Chen *et al.* (2014) experimentally investigated the feasibility of using SMA confinement technique in non-circular sections. In spite of the promising potential of this new SMA confinement technique, there is still very limited experimental data and numerical tools that are pertinent to SMA confined concrete. SMA confinement technique mainly utilizes the shape recovery ability of SMAs upon temperature changes. This unique shape recovery phenomenon enables the stressing of SMA spirals simply through heating. To apply SMA confinement, SMA wire is first prestrained and then wrapped around the RC column as spirals. The SMA spirals are then heated above austenite finish temperature to activate the shape recovery. Due to the constraint from the concrete column, SMA spirals are not able to recover their original shape and therefore recovery stress develops along the SMA spirals, and hence confining pressure is induced. NiTiNb SMA is chosen in this study to ensure that the spiral is able to maintain its recovery stress at a wide range of temperature, due to its sufficiently wide thermal hysteresis that covers the range of expected ambient temperature. It is important to note that SMA confined concrete behavior is unique and different from purely actively or purely passively confined concrete, because in SMA confinement, active confining pressure is applied to concrete prior to loading through activation of shape memory effect, and additional passive confining pressure is applied to concrete during loading due to the deformation sustained by SMA spirals when concrete dilates. Therefore, the behavior of SMA confined concrete is a combination of active and passive confinement, which has not yet been studied in previous research, and therefore more experimental and numerical work is needed to understand this behavior. This study first presents the results of a comprehensive experimental program on SMA spirals confined concrete cylinders, aiming to understand how concrete strength and SMA spiral spacing affect the constitutive behavior of concrete and how stiffness degradation affects the behavior of SMA confined concrete subjected to cyclic loading. Then the experimental results are utilized to develop a plasticity-based constitutive model that is able to capture the cyclic behavior of SMA confined concrete.

2. Experimental Investigation

2.1 Test Specimens and Experimental Program

A total of 20 concrete cylinders with a diameter of 152.4 mm and a height of 305 mm were tested in this study. Table 1 shows the characteristics of all tested specimens. “UC” denotes unconfined specimens, “SMA” denotes SMA confined specimens. B1, B2, B3, B4, and B5 denote concrete batch number. Concrete batches with target 28-day compressive strength ranged between 30.6 MPa and 55.3 MPa were considered in the study. Different levels of active confining pressure ranging between 0.91 MPa and 3.92 MPa were investigated by varying the SMA spiral spacing. S1, S2, S3, S4, and S5 denote the five different levels of active confining pressures, namely, 0.91 MPa, 1.23 MPa, 1.92 MPa, 2.85 MPa and 3.92 MPa, respectively. “C” and “M” denote the loading type: cyclic and monotonic compression, respectively. SMA wires used in the study were already prestrained by the manufacturer to approximately 6% strain with diameters of about 2.0 mm and recovery stress of 607 MPa. To understand the passive confinement behavior of SMA wire, thermally prestressed wires were subjected to uniaxial tensile loading. Test results showed an approximately bilinear behavior of SMA wire with yield stress of 800 MPa, and the ultimate stress was 1270 MPa with an ultimate strain of 20%. Active confining pressures shown in Table 1 were calculated based on the effective confining pressure concept proposed by Mander *et al.* (1988). Note that no internal longitudinal and transverse reinforcement were included in the test in order to put emphasis on the concrete confinement solely and eliminates the overshadowing of the results that could be attributed to internal reinforcement, detailing, and bond-slip, etc. As an example of the tested specimens, Fig. 1

shows specimens with spiral spacing of 25.4 mm, 19.1 mm, 12.7 mm and 6.4 mm, corresponding to confinement levels S1, S2, S3 and S5, respectively. All specimens were loaded using a 2.7 MN hydraulic load frame with a loading/unloading strain rate of 0.5%/min under displacement control. For cyclically loaded specimens, the increment of the first three cycles was 0.1% axial strain, followed by eight cycles of 0.4% strain. After that, the size of increment was adjusted to accommodate the time constraints of the lab. Axial extensometer with a gauge length of 152.4 mm was utilized to measure the concrete axial strain. Six lateral strain gauges with a gauge length of 2 mm were attached to SMA spiral at the mid height of the cylinders, 60° apart from each other in order to monitor the lateral strain development in the wires during loading.

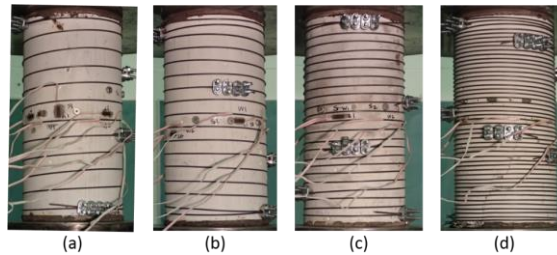


Fig. 1 - Sample of test specimens (a) SMA-B2S1C; (b) SMA-B2S2C; (c) SMA-B2S3C; (d) SMA-B2S5C

2.2 Test Results and Analysis

Figure 2 shows the axial stress-axial strain and axial stress-lateral strain relations obtained under cyclic loading for concrete specimens with concrete strength of 39.6 MPa as an example. The peak stresses of SMA-B2S1C, SMA-B2S2C, SMA-B2S3C, and SMA-B2S5C were 45.1 MPa, 46.0 MPa, 49.3 MPa, and 59.8 MPa, respectively. The peak stress of the SMA confined concrete increased by 13.9%, 16.2%, 24.5%, and 51.0%, respectively compared to that of the unconfined concrete. The ultimate axial strains, at which the first rupture of SMA spirals occurs, of SMA-B2S1C, SMA-B2S2C, SMA-B2S3C, and SMA-B2S5C were 0.0533 mm/mm, 0.0523 mm/mm, 0.0765 mm/mm and 0.1198 mm/mm, respectively and the corresponding ultimate stresses were 32.0%, 41.3%, 48.6% and 81.8% of the peak stresses, respectively. These results confirm that the peak stress and ultimate stress of SMA confined concrete increased as active confining pressure increased. It is worth noting that in some cases the monitoring of lateral strain was terminated earlier than that of axial strain due to damages of strain gauges during testing.

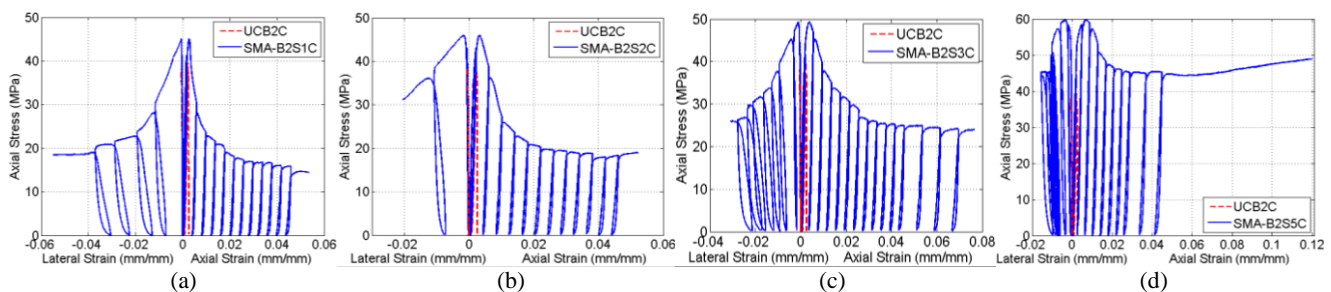


Fig. 2 - Axial stress-axial strain and axial stress-lateral strain relations of concrete with strength of 39.6 MPa and different SMA confinement levels: (a) SMA-B2S1C; (b) SMA-B2S2C; (c) SMA-B2S3C; (d) SMA-B2S5C.

Table 1 summarizes the test results of SMA confined concrete specimens. A transition point is defined to capture one of the key points in the SMA confined concrete stress-strain curve, from which the slope of the descending branch significantly reduces and the change of the slope is minor afterward, which represents the start of the axial stress plateau. Based on experimental data observations, the transition point was chosen to be the point where axial strain reaches a value of 2.5%, and the corresponding stress is defined as residual stress f_{res} . Note that in the table, the lateral strain listed for transition points indicates either the actual lateral strain measured at 2.5% axial strain, or the maximum lateral strain measured in cases where lateral strain gauges were damaged prior to reaching 2.5% axial strain. Average passive confining pressures were calculated based on the lateral strain along the wires and the stress-strain relation of SMA wires. It can be found that in SMA-B1S2C



and SMA-B1S5C, the ratios of the average passive confining pressure to active confining pressure increased from 24.4% to 34.8% as the active confining pressure increased from 1.23 MPa to 3.92 MPa. Similar trend can be found in all other specimens. That means that the effect of active confining pressure is more dominant than passive confining pressure on delaying concrete lateral dilation and increasing concrete strength. It can be also noted that when active confining pressure decreases to a certain limit, it will become less important in the improvement of strength and ductility. Comparing SMA-B2S1C and SMA-B2S2C with active confinement of 0.91 MPa and 1.23 MPa, respectively, the differences on both peak stress and ultimate strain were only 2%. Therefore, 1.23 MPa is considered as a lower bound for effective active confining pressure in the SMA confinement technique.

Table 1- Characteristics and test results summary of all specimens

	Active Confinement (MPa)	f'_{cc} (MPa)	ϵ'_{cc}	f_{ult} (MPa)	ϵ_{ult}	Transition Point		
						f_{res} (MPa)	Lateral Strain	Passive Confinement (MPa)
UC-B1C	0	30.5	0.0016	-	-	-	-	-
SMA-B1S2C	1.23	44.9	0.0027	16.9	0.0663	20.4	0.0278	0.4
SMA-B1S3C	1.92	40.4	0.0035	30.9	0.1005	28.1	0.0134	0.5
SMA-B1S5C	3.92	56.9	0.0057	46.0	0.0530	47.1	0.0068	1.0
UC-B2C	0	39.6	0.0022	-	-	-	-	-
UC-B2M	0	39.6	0.0022	-	-	-	-	-
SMA-B2S1C	0.91	45.1	0.0027	14.4	0.0533	17.4	0.0549	0.4
SMA-B2S2C	1.23	46.0	0.0032	19.0	0.0523	19.7	0.0185	0.4
SMA-B2S3C	1.92	49.3	0.0038	24.0	0.0765	28.9	0.0233	0.6
SMA-B2S5C	3.92	59.8	0.0070	48.9	0.1198	45.6	0.0125	1.1
SMA-B2S2M	1.23	47.4	0.0032	18.4	0.0599	21.8	0.0191	0.4
SMA-B2S3M	1.92	50.7	0.0039	26.4	0.0747	28.5	0.0193	0.6
UC-B3C	0	49.9	0.0022	-	-	-	-	-
SMA-B3S2C	1.23	58.1	0.0031	18.9	0.0585	19.7	0.0385	0.5
SMA-B3S3C	1.92	64.2	0.0037	27.7	0.0958	28.0	0.0243	0.6
SMA-B3S5C	3.92	80.6	0.0056	44.8	0.0641	42.6	0.0056	0.9
UC-B4C	0	36.1	0.0021	-	-	-	-	-
SMA-B4S4C	2.85	51.0	0.0051	34.0	0.0939	37.5	0.0167	0.9
UC-B5C	0	55.4	0.0023	-	-	-	-	-
SMA-B5S4C	2.85	81.6	0.0044	38.0	0.0719	35.7	0.02093	1.0

Figure 3 compares the failure modes of SMA-B2S1C, SMA-B2S2C, SMA-B2S3C, and SMA-B2S5C. SMA spirals confined concrete specimens failed due to the rupture of SMA and showed clear diagonal shear cracks. It can be found from the observation that concrete confined by SMA spirals with smaller spacing experienced more local crushing before SMA spiral ruptured, while with larger spacing, lateral deformation developed faster during loading and the specimen failed due to large shear cracking without too much local damage as shown in SMA-B2S5C. Fig. 4 compares the axial stress-strain envelopes from cyclically loaded SMA confined concrete specimens with different concrete strength but under the same level of active confinement. Fig. 4(a) shows that with SMA confinement, the peak stress of SMA-B1S2C, SMA-B2S2C and SMA-B3S2C increases from that of unconfined concrete by 46.7%, 32.2%, and 86.1%, respectively. However, as the specimens were loaded beyond the peak stress, all three specimens with varying concrete strength reduced to a similar level of residual stress at about 2.5% axial strain (defined earlier as the transition point), and maintained nearly a plateau until reaching the ultimate strain. Similar pattern can be found for other cases with active confinement of 1.92 MPa, 2.85 MPa and 3.92 MPa. It can be concluded that SMA confined concrete with the same active confining pressure reaches a similar level of residual stress at 2.5% axial strain and the ratio between

residual stress and the ultimate stress is within a range of 0.9-1.2, which indicates that active confining pressure is the dominant factor that determines the stress plateau of confined concrete, regardless of the concrete strength.

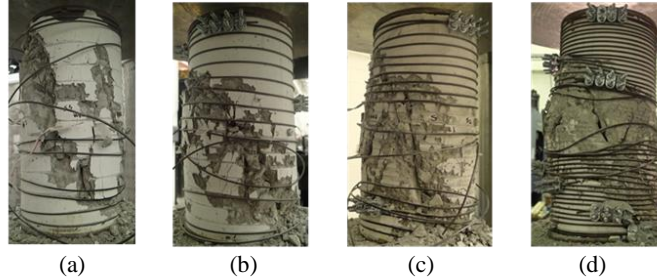


Fig. 3 - Failure modes comparison: (a) SMA-B2S1C; (b) SMA-B2S2C; (c) SMA-B2S3C; (d) SMA-B2S5C.

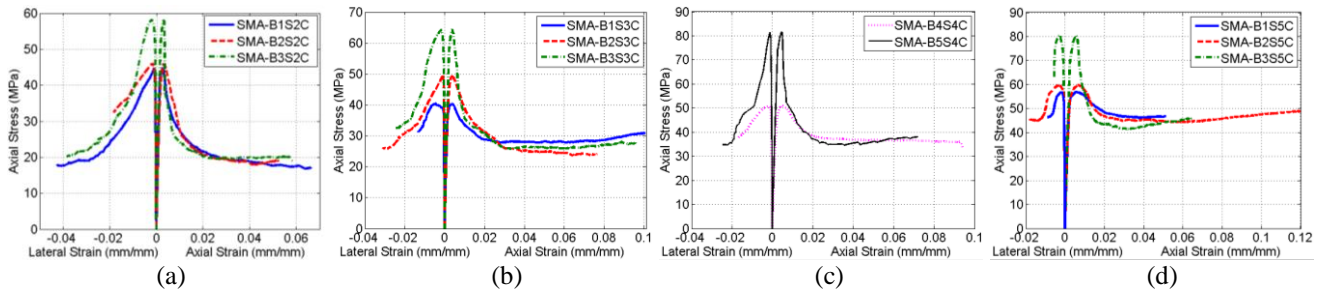


Fig. 4 - Stress-strain envelopes comparison for the same level of active confining pressure and various concrete strengths: (a) 1.23 MPa; (b) 1.92 MPa; (c) 2.85 MPa; and (d) 3.92 MPa.

In order to develop an accurate constitutive model to predict the stress-strain curve of SMA confined concrete, it is important to investigate the characteristics of peak axial stress, residual stress, ultimate stress and their corresponding strain. Regression analyses were conducted to obtain empirical equations that can predict both the peak axial stress and its corresponding axial strain for SMA confined concrete. The suggested equations are shown as Eq. (1) and Eq. (2), with R-square values of 0.76 and 0.96, respectively.

$$f'_{cc} = f'_{co} \left(1 + 6.41 f_{l,active} / f'_{co} \right) \quad (1)$$

$$\varepsilon'_{cc} = \varepsilon_{co} \left(1 + 19.1 f_{l,active} / f'_{co} \right) \quad (2)$$

where, $f_{l,active} / f'_{co}$ denotes the active confinement ratio, which defined as the ratio between active confining pressure $f_{l,active}$ and the unconfined concrete strength f'_{co} ; f'_{cc} and ε'_{cc} are the peak axial stress and its corresponding axial strain; ε_{co} is the axial strain corresponding to the unconfined concrete strength.

As explained earlier, the transition point is one of the key points on the stress-strain curve, which represents the beginning of axial stress plateau. Using regression analysis, Eq. (3) was derived to describe the relationship between residual stress and active confining pressure with an R-square value of 0.98. Similarly, Eq. (4) was derived to predict the ultimate stress as a function of active confining pressure with an R-square value of 0.97. Fig. 5(a) and 5(b) demonstrates that both residual stress and ultimate stress increase linearly as the active confining pressure increases. One of the most considerable advantages of SMA confinement is the potential to significantly improve the ductility and ultimate strain of the concrete. Therefore, ultimate strain is an important parameter for SMA confined concrete behavior. It was found from the test data that the ultimate strain is closely related to the strength degradation, i.e. the ratio between residual stress and peak stress. Fig. 5(c) shows ultimate strain of SMA confined concrete increases as the ratio between residual stress and peak stress increases. As shown in the figure, two of the data points were considered as outliers (SMA-B1S5C and SMA-B3S5C), therefore were not considered in the regression analysis. Based on regression analysis, Eq. (5) was derived to predict the ultimate strain with R-square of 0.88.

$$f_{res} = 9.22 f_{l,active} + 9.73 \text{ (MPa)} \quad (3)$$

$$f_{ult} = 10.43f_{l,active} + 6.25 \text{ (MPa)} \quad (4)$$

$$\varepsilon_{ult} = 0.176 \left(f_{res} / f_{cc}' \right)^{4.229} + 0.057 \quad (5)$$

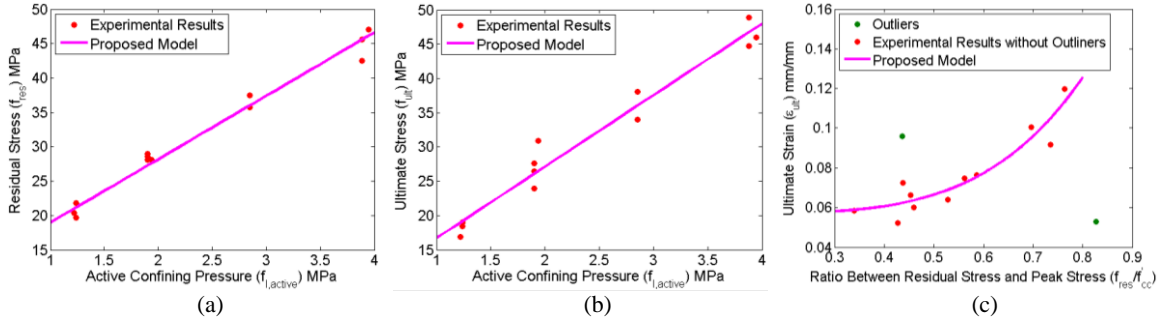


Fig. 5 - Prediction of (a) residual stress, (b) ultimate stress, and (c) ultimate strain.

Since the behavior of SMA confined concrete is a combination of actively and passively confined concrete, it is important to investigate the axial-lateral strain relation of SMA confined concrete in order to better understand its dilation characteristics, so as to understand the passive confining pressure development upon loading. Poisson's ratio is commonly utilized to describe axial-lateral strain relation and for normal unconfined concrete, Poisson's ratio ranges between 0.15 and 0.22 before the concrete reaches about 70% of its strength (Mirmiran and Shahawy 1997). As concrete continues to dilate, dilation ratio increases dramatically, and can reach values greater than 0.5 (Richart *et al.* 1928). Fig. 6 displays the relation between secant dilation ratio, which is the ratio between lateral and axial strain ($\varepsilon_l / \varepsilon_c$), and the normalized axial strain, which is axial strain divided by the axial strain corresponding to the unconfined concrete strength. The number shown in the legend for each specimen is active confinement ratio $f_{l,active} / f_{co}'$. It can be found that for most of the specimen, the secant dilation ratio shows the following features: (1) the initial dilation ratio of confined concrete is similar to that of unconfined concrete; as concrete dilates, it reaches a peak dilation ratio followed by a descending branch; eventually as concrete dilates substantially, it fully relies on the SMA spirals to keep it intact; and then the dilation ratio reaches a plateau; (2) the peak dilation ratio increases as the active confinement ratio decreases; (3) the normalized axial strain at which the SMA confined concrete reaches the peak dilation ratio increases as the active confinement ratio increases. Eq. (6a) was suggested by Mirmiran and Shahawy (1997) to describe secant dilation ratio of confined concrete, which is able to capture the SMA confined concrete dilation characteristics (described by Eqs. 6b - 6d), it is utilized here for the SMA confined concrete secant dilation ratio.

$$\mu = \frac{\mu_0 + \mu_0 c (\varepsilon_c / \varepsilon_{co}) + \mu_{asymptotic} d (\varepsilon_c / \varepsilon_{co})^2}{1 + c (\varepsilon_c / \varepsilon_{co}) + d (\varepsilon_c / \varepsilon_{co})^2} \quad (6a)$$

$$\mu(x = \varepsilon_c / \varepsilon_{co} = 0) = \mu_0, \frac{d\mu(x=0)}{dx} = 0 \quad (6b)$$

$$\mu(x = x_{\mu_{max}}) = \mu_{max}, \frac{d\mu(x = x_{\mu_{max}})}{dx} = 0 \quad (6c)$$

$$\mu(x \rightarrow \infty) = \mu_{asymptotic}, \frac{d\mu(x \rightarrow \infty)}{dx} = 0 \quad (6d)$$

In Eq. (6), $x = \varepsilon_c / \varepsilon_{co}$ denotes the normalized axial strain; μ_0 denotes the initial secant dilation ratio, which is equal to the Poisson's ratio; μ_{max} and $x_{\mu_{max}}$ denote the maximum secant dilation ratio and its corresponding normalized axial strain; $\mu_{asymptotic}$ denotes the asymptotic value of secant dilation ratio as axial strain tends to infinity; c and d are coefficients, which are based on the conditions given in Eqs. (6b) - (6d). The mathematical equations derived from regression analysis are shown as Eqs. (6e) - (6g) with their

corresponding R-square values. It is observed from the test data that all the undetermined parameters in Eq. (6a) depend on the active confinement ratio only; hence the secant dilation ratio can be determined by active confinement ratio and axial strain. Fig. 6 compares the experimental results of secant dilation ratio with the proposed model described in Eq. (6) and it shows that the proposed secant dilation equation is able to capture the lateral and axial strain relation of SMA confined concrete for various concrete strength and active confining pressure values with good agreement.

$$x_{\max} = 31.935 f_{l,active} / f'_{co} + 2.852 \quad (R^2 = 0.994) \quad (6e)$$

$$\mu_{\max} = 0.0462 (f_{l,active} / f'_{co})^{-1.121} \quad (R^2 = 0.926) \quad (6f)$$

$$\mu_{asymptotic} = 1.432 \exp(-14.78 f_{l,active} / f'_{co}) \quad (R^2 = 0.966) \quad (6g)$$

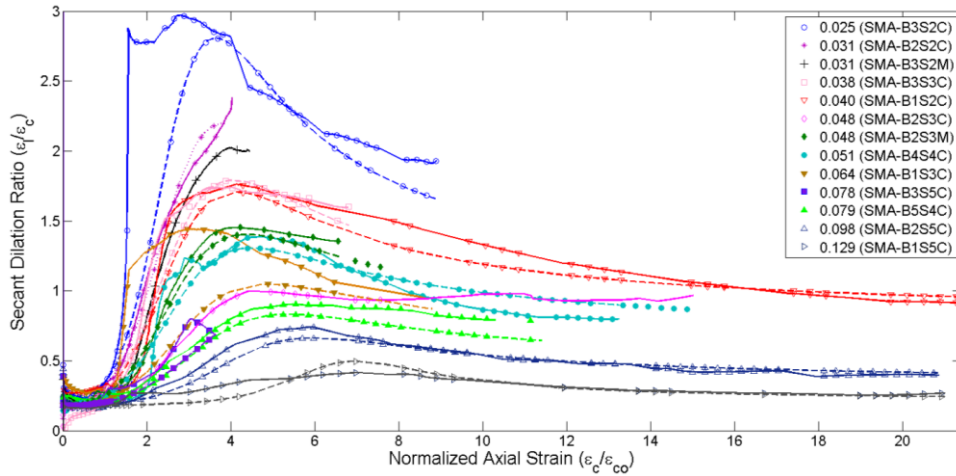


Fig. 6 - Comparison between the experimental (solid) and analytically predicted (dashed) secant dilation ratio.

3. Proposed Plasticity Model

Previous researchers have conducted studies on using plasticity theory to simulate the 3-dimensional behavior of confined concrete (Lubliner *et al.* 1989; Lee and Fenves 1998; Malvar *et al.* 1994). Plasticity models are characterized by three important components, namely, yield criterion, hardening/softening function and flow rule. Yield criterion describes yield surfaces using stress invariants. When the material first reaches the yield surface, plastic deformation is initiated. Hardening/softening function describes the subsequent yield surfaces after first yield. Flow rule determines the magnitude and direction of plastic deformation. These components are based on the multi-axial stress-strain states and for isotropic materials they are described by the principal stresses or the stress invariants to represent the coordinate system independence. In this study, the proposed plasticity model was derived within the framework of Drucker-Prager plasticity model and in order to consider the effect of both the plastic deformation and stiffness degradation on concrete nonlinearity, a damage parameter was also defined. Note that, unless specified, compression is negative and tension is positive in this study.

3.1 Yield Criterion

The Drucker-Prager yield function presented below was utilized in this study:

$$\sqrt{J_2} + \theta I_1 - k = 0 \quad (7)$$

where J_2 and I_1 are the second deviatoric stress invariant and the first stress invariant, respectively; k is the hardening/softening function; θ is the frictional angle, which is a material property that can be derived from experimental results (Chen 1982). For example, this parameter was computed by Richart *et al.* (1928) as 0.2934 for actively confined concrete and by Teng *et al.* (2007) as 0.2634 for fiber reinforced polymer (FRP) confined



concrete. Based on experimental results and regression analysis, θ is equal to 0.3503 for SMA confined concrete.

3.2 Hardening/Softening Function

Hardening/softening function k represents the first and subsequent yield surfaces. It has been proven by several researchers that hardening/softening function of confined concrete depends on concrete strength, lateral confinement and plastic deformation (Oh 2002; Yu *et al.* 2010). As for Drucker-Prager model, hardening/softening function can be calculated using equation $k = \sqrt{J_2} + \theta I_1$. Fig. 7(a) displays a typical shape of hardening/softening function calculated from the test results. It increases linearly starting from an initial value k_0 , and after reaching a peak value k_{peak} , it decreases to a plateau k_{res} . Tsai (1988) recommended an equation [Eq. (8a)] to describe the stress-strain relation of concrete, which can control both the ascending and descending branches of the stress-strain curve. Since the features of hardening/softening function are similar to the axial stress-strain relation of concrete, Eq. (8a) was utilized to describe the hardening/softening function at the pre-plateau range, with slight modification to account for the initial value k_0 . After reaching the residual value k_{res} , the hardening/softening value is assumed to be constant.

$$Y = \frac{mX}{1 + \left(m - \frac{n}{n-1}\right)X + \frac{X^n}{n-1}} \quad (8a)$$

In Eq. (8a), $Y = k / k_{peak}$; $X = \hat{\varepsilon}^p / \hat{\varepsilon}_{k,peak}^p$; k_{peak} is the peak value in the hardening/softening function; $\hat{\varepsilon}^p$ is the equivalent plastic strain, which represents the 3-D plasticity accumulation in concrete, and the incremental equivalent plastic strain is defined as $\Delta\hat{\varepsilon}^p = \sqrt{\Delta\varepsilon_c^p + \Delta\varepsilon_l^p + \Delta\varepsilon_t^p}$, in which $\Delta\varepsilon_c^p$ and $\Delta\varepsilon_l^p$ are the incremental axial and lateral plastic strain; $\hat{\varepsilon}_{k,peak}^p$ is the equivalent plastic strain at the peak of hardening/softening function; parameter $m = \partial Y / \partial X = E_0^k / E_p^k$ controls the ascending slope; parameter n controls the descending slope; E_0^k defines the initial slope of the hardening/softening function, and $E_p^k = k_{peak} / \hat{\varepsilon}_{k,peak}^p$. Parameters E_0^k , k_0 , k_{peak} , $\hat{\varepsilon}_{k,peak}^p$, k_{res} , and n were derived using regression analysis based on the experimental results and they can be calculated using Eqs. (8b) - (8g). It should be noted that although hardening/softening function is written as a function of equivalent plastic strain, the effect of concrete strength and SMA confinement on the hardening/softening function is represented in the parameters mentioned above.

$$E_0^k = -270433 f_{l,active} / f_{co}' + 45972 \text{ (MPa)} \quad (R^2 = 0.834) \quad (8b)$$

$$k_0 = (-0.6958 f_{l,active} / f_{co}' + 0.1071) \cdot (-f_{co}') \text{ (MPa)} \quad (R^2 = 0.824) \quad (8c)$$

$$k_{peak} = 0.266(-f_{co}') \text{ (MPa)} - 1.421 \quad (R^2 = 0.876) \quad (8d)$$

$$\hat{\varepsilon}_{k,peak}^p = (7.461 f_{l,active} / f_{co}' + 1.036) \cdot (-\varepsilon_{co}') \quad (R^2 = 0.795) \quad (8e)$$

$$k_{res} = 0.7255(-f_{l,active}') \text{ (MPa)} + 1.077 \quad (R^2 = 0.913) \quad (8f)$$

$$n = 0.0144(-f_{co}') \text{ (MPa)} + 1.582 \quad (R^2 = 0.795) \quad (8g)$$

3.3 Flow Rule

A non-associated flow rule was utilized in the proposed model, which depends on concrete strength, plastic deformation and lateral confining pressure. The incremental equivalent plastic strain can be described by Eq. (9a) and a Drucker-Prager type potential function G is utilized [Eq. (9b)].



$$\Delta \hat{\varepsilon}^p = \Delta \lambda \sqrt{\frac{\partial G}{\partial \sigma_i} \frac{\partial G}{\partial \sigma_i}} \quad (i=1,2,3) \quad (9a)$$

$$G = \sqrt{J_2} + \psi I_1 \quad (9b)$$

In Eq. (9), ψ is potential function parameter to be determined based on the plastic deformation characteristics; $\Delta \lambda$ denotes the magnitude of plastic deformation in the direction of $\partial G / \partial \sigma_i$, in which σ_i is the principal stress of concrete in the direction i . Dilation rate α was used to describe the potential flow for confined concrete, which represents the relation between incremental volumetric strain and the incremental deviatoric strain. Dilation rate α can be calculated based on axial stress-axial strain relation, axial strain-lateral strain relation, using Eq. (10) (Oh 2002; Yu *et al.* 2010).

$$\alpha = \frac{\Delta I_1^p}{\Delta \sqrt{J_2^p}} = \sqrt{3} \frac{\Delta \varepsilon_c^p + 2\Delta \varepsilon_l^p}{|\Delta \varepsilon_c^p - \Delta \varepsilon_l^p|} = \sqrt{3} \frac{1 + 2\Delta \varepsilon_l^p / \Delta \varepsilon_c^p}{\Delta \varepsilon_l^p / \Delta \varepsilon_c^p - 1} = 6\psi \quad (10)$$

where, ΔI_1^p is the incremental volumetric plastic strain; ΔJ_2^p is the incremental second deviatoric plastic strain; $\Delta \varepsilon_c^p$ and $\Delta \varepsilon_l^p$ are the incremental axial and lateral plastic strain. Fig. 7(b) shows a typical shape of the dilation rate function from the experimental results. Similar to the hardening/softening function, the dilation rate function increases linearly starting from an initial value α_0 , and after reaching a peak value α_{peak} , it decreases to a plateau α_{res} . To represent this behavior, Eq. (11a) was chosen to describe the dilation rate function at the pre-plateau stage. After reaching the residual value α_{res} , the dilation rate value was assumed to be constant.

$$U = \frac{pV}{1 + \left(p - \frac{q}{q-1} \right) V + \frac{V^q}{q-1}} \quad (11a)$$

In Eq. (11a), $U = (\alpha - \alpha_0) / (\alpha_{peak} - \alpha_0)$; $V = \hat{\varepsilon}^p / \hat{\varepsilon}_{\alpha,peak}^p$; $\hat{\varepsilon}_{\alpha,peak}^p$ is the equivalent plastic strain at the peak of dilation rate function; $p = \partial U / \partial V = E_0^\alpha / E_p^\alpha$, which controls the ascending slope; and q controls the descending slope; E_0^α is the initial slope of the dilation rate function; $E_p^\alpha = (\alpha_{peak} - \alpha_0) / \hat{\varepsilon}_{\alpha,peak}^p$. The initial dilation rate α_0 can be calculated using Eq. (11a) by substituting Poisson's ratio $\nu = -\Delta \varepsilon_l^p / \Delta \varepsilon_c^p = 0.18$, one can obtain $\alpha_0 = -0.9394$. Parameters E_0^α , α_{peak} , $\hat{\varepsilon}_{\alpha,peak}^p$, α_{res} , and q were derived using regression analysis based on the test data, and they can be calculated using Eq. (11b) - (11f).

$$E_0^\alpha = \begin{cases} -11722 f_{l,active} / f_{co}' + 1417.3 \text{ (MPa)} & (f_{l,active} / f_{co}' \leq 0.1) \\ 245.1 \text{ (MPa)} & (f_{l,active} / f_{co}' > 0.1) \end{cases} \quad (R^2 = 0.770) \quad (11b)$$

$$\alpha_{peak} = \frac{0.1357}{(f_{l,active} / f_{co}' + 0.0261)} \quad (R^2 = 0.980) \quad (11c)$$

$$\hat{\varepsilon}_{\alpha,peak}^p = \frac{(-\varepsilon_{co}) (3.708 f_{l,active} / f_{co}' + 0.0212)}{(f_{l,active} / f_{co}' - 0.0118)} \quad (R^2 = 0.948) \quad (11d)$$

$$\alpha_{res} = -16.468 f_{l,active} / f_{co}' + 1.176 \quad (R^2 = 0.993) \quad (11e)$$

$$q = \begin{cases} -111.6 f_{l,active} / f_{co}' + 8.464 & (f_{l,active} / f_{co}' < 0.04) \\ 4 & (f_{l,active} / f_{co}' \geq 0.04) \end{cases} \quad (R^2 = 0.961) \quad (11f)$$

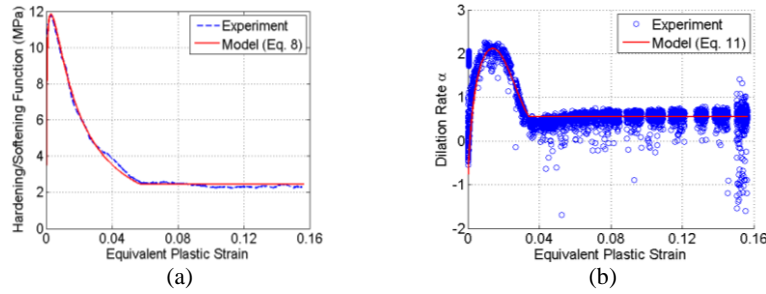


Fig. 7 - Comparison of experimental and modeling (a) hardening/softening function; (b) dilation rate function, for specimen SMA-B3S3C.

3.4 Damage Parameter

Modeling both damage and plasticity accumulation is important to simulate the nonlinear stress-strain behavior of SMA confined concrete as mentioned previously. In order to capture the unloading and reloading stiffness of SMA confined concrete, it is essential to define a damage parameter, which is derived based on the stiffness degradation during cyclic loading. Based on experimental observations, the following assumptions were made for the proposed model: (1) unloading and reloading stiffness is the same; (2) stress and strain are linearly related between unloading and reloading points. Damage parameter can be calculated as $d = 1 - E_r / E_0$, where E_r is the reloading stiffness of SMA confined concrete at a certain axial strain and E_0 is the elastic modulus of the concrete. It is found that the stiffness of SMA confined concrete decreases logarithmically as axial strain increases and the degradation rate solely depends on the active confining pressure, regardless of concrete strength. Therefore, the logarithmic function shown as Eq. (12a) was utilized to model the damage parameter. Parameters a and b were obtained using curve fitting for each confinement level. Therefore, parameters a and b can be calculated using Eq. (12b) and Eq. (12c) based on regression analysis. Fig. 8 compares the proposed model with experimental results of damage parameter, and demonstrates that the proposed model can closely predict the stiffness degradation of SMA confined concrete under cyclic loading.

$$d = 1 - E_r / E_0 = -a \ln(\varepsilon_c) + (1 - b) \quad (12a)$$

$$a = 0.0085 f_{l,active} (MPa) - 0.1717 \quad (R^2 = 1.0) \quad (12b)$$

$$b = -a \ln(0.1764 f_{l,active} (MPa) + 0.0082) \quad (R^2 = 1.0) \quad (12c)$$

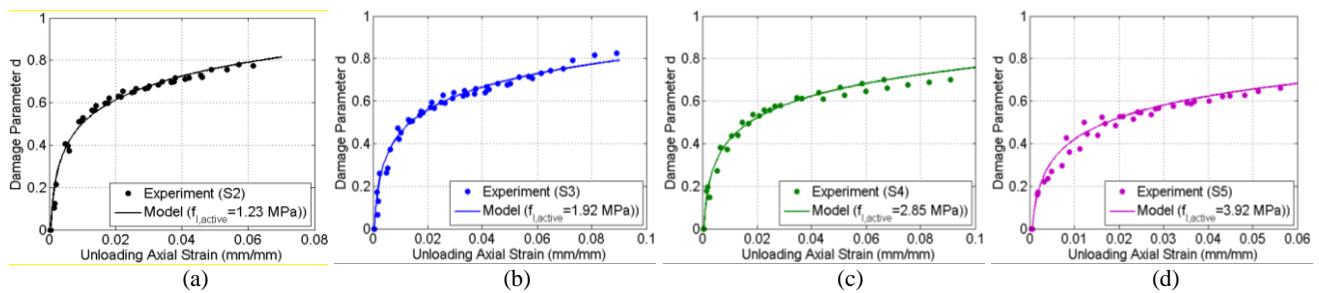


Fig. 8 - Comparison of the damage parameter model prediction and the experimental results under various active confining pressures of: (a) 1.23 MPa; (b) 1.92 MPa; (c) 2.85 MPa; (d) 3.92 MPa.

4. Comparison of Proposed Model and Experimental Results

To examine whether the proposed constitutive model is capable of capturing the SMA confined concrete behavior, the numerical results were compared with the experimental results. Fig. 9 compares the experimental and numerical results from the proposed model for both the axial stress-axial strain and axial stress-lateral strain behaviors of specimens SMA-B2S2C, SMA-B2S3C, and SMA-B2S5C as examples. It shows that the proposed plasticity model was able to simulate the stress-strain relation of SMA confined concrete with good agreement.

Table 2 shows the ratios between experimental and numerically predicted results for peak axial stress, and its corresponding axial strain, ultimate stress and its corresponding ultimate strain, as well as the axial stress at 2.5% axial strain (residual stress). The average prediction to experiment ratios of peak stress, ultimate stress and axial stress at 2.5% are 0.998, 1.028, and 0.985, respectively, with standard deviation no more than 6.5%. The relatively high average error (12.6%) of the ultimate strain came from two specimens, SMA-B1S5C and SMA-B3S3C, which have been identified as outliers as explained earlier. The average error reduces to 0.7%, when excluding these two outliers. Although the average prediction to experiment ratio of peak strain is relatively high, the error in the prediction is minor when the absolute value is considered. Therefore, the proposed model has verified to be in good agreement with the experimental results and is deemed able to capture the NiTiNb SMA confined stress-strain behavior for both axial and lateral directions under cyclic loading.

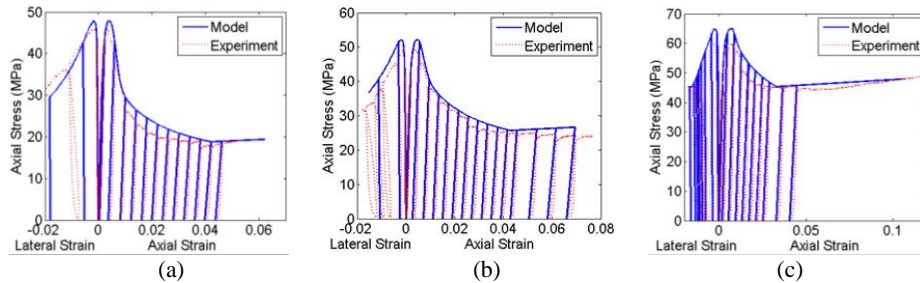


Fig. 9 - Comparison of axial stress-axial strain and axial stress-lateral strain experimental and numerical results using the proposed model for specimens: (a) SMA-B2S2C; (b) SMA-B2S3C; (c) SMA-B2S5C.

Table 2 - Ratios between plasticity model predictions and experimental results

	Strength (MPa)	Pitch (mm)	Peak Stress	Peak Strain	Ultimate Stress	Ultimate Strain	Axial Stress @ 2.5%
SMA-B1S2C		15.9	0.823	1.278	1.118	1.048	0.929
SMA-B1S3C	30.6	10.2	1.024	1.157	0.872	0.852	0.957
SMA-B1S5C		5.1	0.949	1.014	1.038	2.840	1.015
SMA-B2S2C		19.1	1.042	1.255	1.021	1.190	0.985
SMA-B2S3C	39.6	12.7	1.057	1.205	1.112	0.910	0.921
SMA-B2S5C		6.4	1.086	1.036	0.980	0.895	1.051
SMA-B3S2C		19.1	1.035	1.308	1.042	1.009	0.999
SMA-B3S3C	50.0	12.7	1.001	1.182	0.971	0.655	0.958
SMA-B3S5C		6.4	0.956	1.073	1.080	1.322	1.136
SMA-B4S4C	36.1	7.6	1.022	0.984	1.085	1.016	0.984
SMA-B5S4C	55.3	7.6	0.941	1.174	0.981	0.937	1.044
SMA-B2S2M		19.1	1.010	1.239	1.052	1.039	0.890
SMA-B2S3M	39.6	12.7	1.025	1.216	1.009	0.931	0.935
Average			0.998	1.620	1.028	1.126	0.985
Standard Deviation			0.065	1.560	0.065	0.518	0.063

5. Conclusion

This study first focused on experimentally investigating the behavior of SMA confined concrete. Uniaxial compressive tests were conducted on cylinders confined with five different SMA spiral spacing and with active confining pressures ranging from 0.91 to 3.92 MPa. Next, experimental results were utilized to derive a new plasticity-based constitutive model that can accurately simulate the axial stress-axial strain and axial stress-lateral strain behaviors of SMA confined concrete. The following conclusions can be drawn from this study: (1) the effectiveness of SMA confinement on strength and ductility enhancement increases as active confining pressure increases; (2) the effect of SMA confinement was observed under SMA active confining pressure as



low as 1.23 MPa; (3) this study was able to derive equations to predict the peak stress and its corresponding peak strain, residual stress, ultimate stress, and ultimate strain of SMA confined concrete; (4) residual stress and ultimate stress of SMA confined concrete are independent of concrete strength and are functions of active confining pressure only; (5) a Drucker-Prager type plasticity model was utilized to describe 3-dimensional constitutive behavior of SMA confined concrete. Both the hardening/softening functions and the dilation rate functions were developed as functions of equivalent plastic strain, and both were able to capture the effect of concrete strength and SMA confinement; (6) through comparing the experimental results with the proposed plasticity model predictions, it proved that the proposed model was able to capture the axial stress-axial strain, axial stress-lateral strain behavior of SMA confined concrete accurately including peak stress (0.2% error on average), axial stress at 2.5% strain (1.5% error on average), ultimate stress (2.8% error on average), ultimate strain (0.7% error on average), as well as the stiffness changes during cyclic loading.

6. Acknowledgements

The authors acknowledge the financial support provided for this research from the National Science Foundation through its Faculty Early Career Development (CAREER) program under Award No. 1055640.

7. References

- [1] Richart FE, Brandtzaeg A, Brown, RL (1928): A study of the failure of concrete under combined compressive stresses. *Technical Report Bulletin No. 185*, Engineering Experiment Station, University of Illinois, Urbana.
- [2] Sheikh SA, Uzumeri SM (1982): Analytical model for concrete confinement in tied columns. *J. Struct.*, **108** (12), 2703-2722
- [3] Mander JB, Priestley MJN, Park R (1988): Theoretical stress-strain model for confined concrete. *J. Struct. Eng.*, **114** (8), 1804-1826.
- [4] Imran I, Pantazopoulou SJ (1996): Experimental study of plain concrete under triaxial stress. *ACI Mater. J.*, **93** (6), 589-601.
- [5] Andrawes B, Shin M (2008): Seismic retrofitting of bridge columns using shape memory alloys. *Proc. SPIE - The International Society for Optical Engineering*, Volume 6928.
- [6] Shin M, Andrawes B (2011): Lateral cyclic behavior of reinforced concrete columns retrofitted with shape memory spirals and FRP wraps. *J. Struct. Eng.*, **137** (11), 1282-1290.
- [7] Chen Q, Shin M, Andrawes B (2014): Experimental study of non-circular concrete elements actively confined with shape memory alloy wires. *Constr. Build. Mater.*, **61**, 303-311.
- [8] Mirmiran A, Shahawy M (1997): Dilation characteristics of confined concrete. *Mech. Cohes. Frict. Mat.*, **2** (3), 237-249.
- [9] Lubliner J, Oliver J, Oller S, Onate E (1989): A plastic-damage model for concrete. *Int. J. Solid Struct.*, **25** (3), 299-326.
- [10] Lee J, Fenves GL (1998): Plastic-damage model for cyclic loading of concrete structures. *J. Eng. Mech.*, **124** (8), 892-900.
- [11] Malvar LJ, Crawford JE, Wesevich JW, Simons D (1994): A new concrete material model for DYNA3D. *Technical Report TR-94-14.3*, Karagozian & Case.
- [12] Chen WF (1982): *Plasticity in Reinforced Concrete*. J. Ross Publishing.
- [13] Teng J, Huang Y, Lam L, Ye L (2007): Theoretical model for fiber reinforced polymer confined concrete. *J. Compos. Constr.*, **11** (2), 201-210.
- [14] Oh B (2002): A plasticity model for confined concrete under uniaxial loading. Ph.D. thesis, Lehigh University.
- [15] Yu T, Teng JG, Wong YL, Dong SL (2010): Finite element modeling of confined concrete-I: Drucker-Prager type plasticity model. *Eng. Struct.*, **32** (3), 665-679.
- [16] Tsai, W. (1988): Uniaxial compressional stress-strain relation of concrete. *J. Struct. Eng.*, **114** (9), 2133-2136.